Advances in Intelligent Systems Research, volume 175
2nd International Conference on Industry 4.0 and Artificial Intelligence (ICIAI 2021)

PANI-CSA/Co_3O_4 Nanocomposite Films: Optical, Morphological, and Structural Properties

Mahmoud Al-Gharram[a], Inshad Jum'h[a,*], Ahmad Telfah[c,d], Mahmoud Al-Hussein[b,d]

[a] *School of Basic Sciences and Humanities, German Jordanian University (GJU), Amman,*
[b] *Physics Department, The University of Jordan, Amman, 11942, Jordan*
[c] *Leibniz-Institut für Leibniz-Institut für Analytische Wissenschaften-ISAS, Dortmund, Germany.*
[d] *Hamdi Mango Center for Scientific Research, The University of Jordan, Amman, 11942, Jordan*

[*] *Corresponding author. Email: inshad.yousef@gju.edu.jo*

ABSTRACT

Nanocomposites films of (PANI-CSA)/(Co_3O_4 NPs) with (1, 3, 6, and 12 wt.%) of Co_3O_4 NPs were deposited on ITO-glass substrates using the electrochemical polymerization method. The optical properties and parameters of the nanocomposites films were investigated and determined through experimental UV-Vis spectra. Adding Co3O4 NPs to the nanocomposite film lowers the π -polaron bandgap and the π-π*. The observed optical properties reveal the potential of these nanocomposite films as active materials in novel optical and electromagnetic devices. Additionally, the crystallography and structural evolution of the nanocomposites films with changing Co_3O_4 NPs were investigated by employing SEM and XRD.

Keywords: *Polyaniline, Cobalt oxide, Camphor sulfonic acid, Electro- polymerization, Nanocomposites.*

1. INTRODUCTION

Cobalt(II, III) oxide (Co_3O_4) is an antiferromagnetic solid oxide that is classified as a ferrite of the spinel-type and can be synthesized in nanoparticles (NPs) form with higher catalytic activity and remarkable optical and magnetic properties and they have promising applications in memory devices, electrical switching and microwave devices and sensors [1]. Nanocomposites of organic/inorganic exhibit integral properties between the organic and the inorganic material [2]. Conducting polymers are used in various applications, including optics [3], electronics, actuators, and sensors [4]. Their conductivity can be enhanced significantly by doping with the appropriate dopants [5]. Polyaniline (PANI) considered as the most essential conductive polymer because of its relative ease of preparation, good physical and chemical stability, tuneable optical energy gap, and electrical conductivity [6]. In this work, nanocomposite films of PANI protonated with camphor sulfonic acid (CSA) and doped with Co_3O_4 NPs formulated by employing an in situ electrochemical deposition method with different concentrations of Co_3O_4 NPs forming (PANI-CSA)/(Co_3O_4 NPs). Nanocomposite films were deposited on an ITO-glass substrate and characterized by scanning electron microscopy (SEM) and X-ray diffraction (XRD) analysis. Furthermore, optical properties were investigated, and optical parameters were determined using UV-Vis spectroscopy. (PANI-CSA)/(Co_3O_4 NPs) nanocomposite films are proposed to serve as an optical sensor in the visible light range based on their unique and tuneable optical parameters such as their refractive indices and absorbance in the wavelengths from 300 to 600 nm.

2. EXPERIMENTAL PROCEDURE

Aniline ($C_6H_5NH_2$) and camphor sulfonic acid (CSA) ($C_{10}H_{16}O_4S$), and deionized water (DIW) were purchased from Sigma-Aldrich Co. Ltd. Indium tin oxide (ITO) coated glass substrates were provided by Ossila Ltd. provided Co_3O_4 nanoparticles were purchased from US Research Nanomaterials Inc. They were in the 15 nm average size.

The ITO-glass substrates with an area of 13.75 cm^2 were cleaned before the deposition. The electrolyte solution was composed of polyaniline protonated with CSA (PANI-CSA) was prepared by dissolving 0.2 M aniline

and to 0.35 M CSA in 25 ml DIW at room temperature (293 K) under stirring for 10 minutes. The solution of PANI-CSA in DIW was mixed with 0, 1, 3, 6, and 12 wt.% of Co_3O_4 NPs with respect to aniline, where every ratio was deposited in separated electrochemical measurement. Nanocomposite films were electrodeposited in a bipolar electro-polymerization cell at constant potentials using an Autolab potentiostat (Figure 1). Distance between the ITO-glass (the working electrode) and the counter electrode (high-quality stainless steel) was attained using a 1cm PTFE (Teflon) spacer. The deposited films were let dried in an oven for 2 hours at 45 °C. The average thickness of the nanocomposite films estimated from the SEM micrograph measured at the edge was about 900 nm.

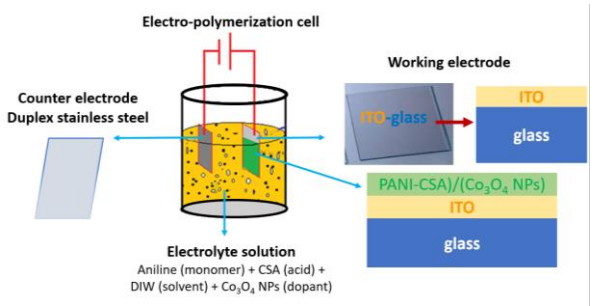

Figure 1. The diagram of electrochemical polymerization cell that used for forming and depositing (PANI-CSA)/(Co_3O_4 NPs) on ITO-glass substrate [17].

(Shimadzu-100) spectrophotometer was employed to acquire UV-Vis spectra in the wavelengths range from 250 to 700 nm. Inspect F50 scanning electron microscope (SEM) was used to investigate and evaluate SEM micrographs. X-ray diffractometer (Shimadzu X-ray diffractometer Model: 7000) was used to identify the crystalline structure, using Cu K radiation (=1.5418), at 40 kV and 40 mA.

3. RESULTS AND DISCUSSION

UV-Vis transmittance, reflectance, and refractive index of the nanocomposite films are shown in Figure 2a. Nanocomposite films are transparent in visible light (T%= 50-80). Moreover, showing a similar pattern regardless of the Co_3O_4 NPs content. However, a significant reduction in transmittance correlated to the increase in Co_3O_4 NPs concentration.

The absorbance spectra show two overlapped and distinct absorption peaks at 375 and 440 nm, as shown in Figure 2c. Additionally, a free carrier tail appears from 515 nm to the near-infrared (NIR) region suggests polaron band delocalization. The shallow peak at 375 *nm* is attributed to the π* transition inside the benzoind (B) ring, while the strong peak at 440 nm is ascribed to the localized polarons (polaron-π*) (quinoid, Q) transition [8]. The mentioned peaks overlapping shows the wide dispersion of the polaron-π* evolution.

Despite the spectra of all nanocomposite films demonstrating the same primary trend, but the peaks of they are somewhat shifted to higher wavelengths (red-shift), these modest red changes in band locations are caused by the interaction of the PANI-CSA chains with the Co_3O_4 NPs and indicate a reduction in optical bandgaps (E_g). The inclusion of Co_3O_4 NPs lowered the deduced refractive index (n) value while the overall trend of the PANI-CSA film was invariant. The Co_3O_4 NPs (6 or 12 wt.%) split the broad peak into two peaks at 303 and 346 nm. The n of all nanocomposites films were in the range (1.90-2.13) for PANI-CSA and (1.78-2.10) for (PANI-CSA)/(Co_3O_4 NPs), respectively. At roughly 300 nm, (PANI-CSA)/(Co_3O_4 NPs) (6 and 12 wt.%) and PANI-CSA (1 and 3 wt.%) exhibit the first absorption bands corresponding to the π* transition. A second absorption band at the concentration (6 and 12 wt.%) is due to optical transitions (direct) from upper occupied band to the polaron band (HOMO). The third is induced by direct optical transitions from the highest upper occupied level to the polaron band at 500 nm (-polaron). The optical bandgap of the deposited layers was calculated according to the method in literature [9]. Figure 2 (a and b) shows the curve of $(\alpha h\nu)^2$ vs. photon energy ($h\nu$) for all films. Remarkably, all nanocomposite films followed two significant tendencies.

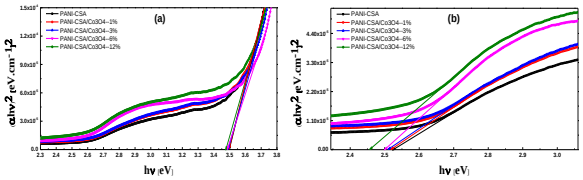

Figure 2: Tauc plot performed on the UV-Vis data acquired of PANI-CSA and PANI-CSA/Co_3O_4 nanocomposite films showing the behavior of inter-band transitions (a) E_{g1} and (b) E_{g2}.

Abound electron-hole pair is generated when the first intercept (E_{g1}) varies between 2.45 and 2.52 eV. In the HOMO–LUMO gap, the lowest energy of a separated, uncorrelated free electron and hole is calculated.

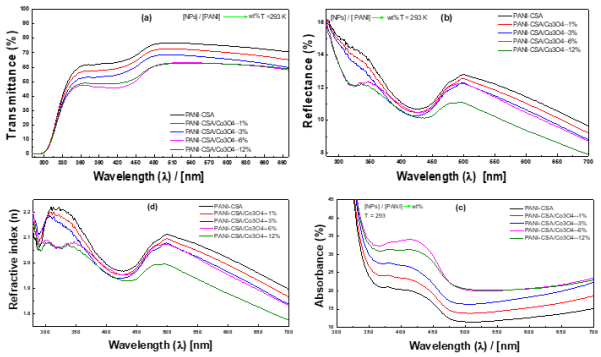

Figure 3. (a) transmittance, (b) reflectance, (c) refractive index (*n*), and (d) absorbance spectra of all films.

The Tauc plot shows two optical bandgaps of PANI-CSA film of 2.52 and 3.50 eV. The first absorption band is

assigned to the polaron transition (quinoid, Q), whereas the second absorption band is attributed to the benzenoid (B) ring π*electron transition. These findings are similar to previously reported PANI-CSA values [11, 12, 13]. PANI-CSA has low E_g values due to a prolongation of the PANI conjugated chain. According to the UV-Vis results in Figure 2, Co_3O_4 NPs to the nanocomposite film decreased the polaron bandgap and the π* band, from 2.51 at 1 wt.% to 2.50 at 3 wt.%, 2.49 at 6 wt.%, and 2.45 eV at 12 wt.%. Table 1 shows the variation of the first energy bandgap E_{g1}, the second energy bandgap E_{g2} of (PANI-CSA)/(Co_3O_4 NPs) nanocomposite films as a function of NPs content.

Table 1: Optical energy bandgaps (E_g) of (PANI-CSA)/(Co_3O_4 NPs) nanocomposite films.

Films and ration	E_{g1} (eV)	E_{g1} (eV)
PANI-CSA	2.52	3.51
(PANI-CSA)/(Co_3O_4 NPs) -1 wt.%	2.51	3.50
(PANI-CSA)/(Co_3O_4 NPs) -3 wt.%	2.50	3.49
(PANI-CSA)/(Co_3O_4 NPs) -6 wt.%	2.49	3.48
(PANI-CSA)/(Co_3O_4 NPs) -12 wt.%	2.45	3.47

SEM micrographs of the nanocomposite films are illustrated in Figure 4 PANI-CSA thick fiber-like formations seemed to cover the whole substrate, as seen in Figure 4a. SEM micrographs at Co_3O_4 NP concentration of 6 wt.% (figure 3b) exhibited a more rod-like structural distribution and more order and crystallinity than in the PANI-CSA films, confirmed by XRD data from the same sample. SEM micrographs of the PANI-CSA/Co_3O_4 at a 12 wt.% (Figure 4c) display very dense nanofibers.

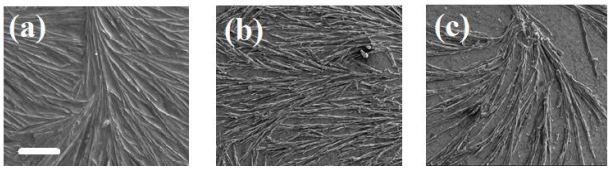

Figure 4. SEM micrographs of the (PANI-CSA)/(Co_3O_4 NPs) nanocomposite films. (a) 0 wt.%, (b) 6 wt.%, and (c) 12 wt.%.

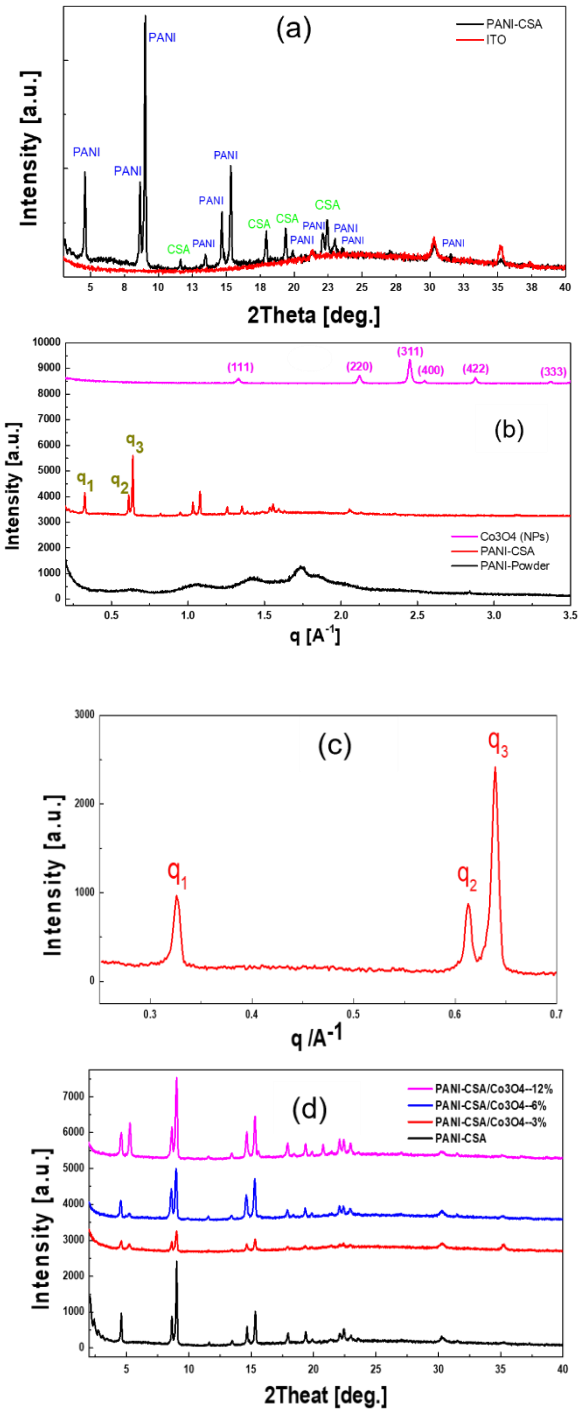

Figure 5: (a) XRD patterns of PANI-CSA film and ITO substrate. (b) XRD patterns of PANI powder, Co_3O_4 NPs, and PANI-CSA film (c) XRD patterns of the first three peaks, (d) XRD patterns of the (PANI-CSA)/(Co_3O_4 NPs) nanocomposite films.

Figure 5 shows the XRD patterns of (PANI-CSA)/(Co_3O_4 NPs) films. XRD pattern of PANI-CSA shows strong peaks, indicating it is highly crystalline following earlier observations [14], where the significant height between 15° and 37° is due to amorphous film sections. On the left are pure Co_3O_4 nanoparticles, PANI powder, and deposition PANI-CSA film. The Co_3O_4 NPs curve shows

typical spinel structure reflections. According to prior research [15, 16], the PANI powder sample displays many prominent peaks overlaid on a diffuse background, but the height at plot A in the PANI powder curve blends into the ground. Another new rise at plot A is evident, and the amorphous phase diffused set much decreased, indicating high crystalline content [17] (a) The X-ray diffraction patterns of the first three peaks for PANI-CSA film match [17]. The second peak is not double the first peak (Table 2 [18, 19]) in Figure 5 (a, b, c and d). Despite this, the third peak is near the second-order location of the first peak (Figure 4b: X-ray diffraction patterns of (PANI-CSA)/(Co_3O_4 NPs) nanocomposite films) (c). At 6% crystallinity, the average crystalline grain diameters (D) and crystallinity of PANI-CSA and nanocomposites are shown in Table 3. Finally, for all nanocomposites, the peaks in the PANI-CSA films were comparable. Nonetheless, they were shifted to the left, and their intensity fluctuated, suggesting coexistence, incorporation, and interaction between the NPs and the PANI-CSA. Adding 3 wt.% Co_3O_4 NPs resulted in a substantial decrease in all crystalline peaks, showing that the PANI-CSA has a lower degree of crystallinity. Increasing the concentration of Co_3O_4 NPs, on the other hand, induces a rise in crystalline peaks in the PANI-CSA film.

Table 2: X-ray curves: Positions of the first and second peaks.

Film and ration	q_1 (A^{-1})	q_2 (A^{-1})	q_3 (A^{-1})	$2q_1$ (A^{-1})
PANI-CSA	0.326	0.614	0.640	0.652
(PANI-CSA)/(Co_3O_4 NPs) - 3 wt.%	0.328	0.614	0.640	0.656
(PANI-CSA)/(Co_3O_4 NPs) - 6 wt.%	0.324	0.612	0.638	0.648
(PANI-CSA)/(Co_3O_4 NPs) - 12 wt.%	0.327	0.614	0.641	0.654

The Williamson–Hall plot (W-H) technique was used to determine the average crystalline grain diameters (*D*) and crystallinity of the PANI-CSA and the nanocomposite film at 12 wt.% are in Table 3.

Table 3: Average crystalline grain and crystallinity of (PANI-CSA)/(Co_3O_4 NPs) nanocomposite film at 12 wt.% of Co_3O_4 NPs.

Film	Average grain size (D) [nm]	Crystallinity [%]
PANI-CSA	61	22.8
(PANI-CSA)/(Co_3O_4 NPs)	57	27.5

4. CONCLUSIONS

Nanocomposite films of (PANI-CSA)/(Co_3O_4 NPs) with (0, 3, 6, 12 wt.%) of Co_3O_4 NPs were prepared by using electrochemical polymerization technique on ITO-glass substrates. The optical, morphological, and electrical properties of the prepared nanocomposite thin films have been investigated. SEM micrographs show, Interestingly, that all films at 12 wt.% NPs concentration exhibit very dense nanofibers. The deduced refractive index and optical band gap energies of the nanocomposite films were tunable with correlation to the Co_3O_4 NPs concentration showing that the system can be used as an optical sensor in the visible light range.

REFERENCES

[1] M. Ghosh, E.V. Sampathkumaran and C.N.R. Rao, Chem. Mater., 17 (2005) 2348.

[2] Jum'h, Inshad, Marwan S. Mousa, Mahmoud Mhawish, Suhad Sbeih, and Ahmad Telfah. "Optical and structural properties of (PANI-CSA-PMMA)/NiNPs nanocomposites thin films for organic optical filters." Journal of Applied Polymer Science 137, no. 18 (2020): 48643.

[3] J. H. Harreld, B. Dunn, and J.I. Zink, J, Effects of organic and inorganic network development on the optical properties of ORMOSILs, Mater. Chem., 7, 1511(1997).

[4] Telfah, Ahmad, Mousa M. Abdul-Gader Jafar, Inshad Jum'h, Mais Jamil A. Ahmad, Jörg Lambert, and Roland Hergenröder. "Identification of relaxation processes in pure polyethylene oxide (PEO) films by the dielectric permittivity and electric modulus formalisms." Polymers for Advanced Technologies 29, no. 7 (2018): 1974-1987.

[5] Alsaad, A. M., Qais M. Al-Bataineh, A. A. Ahmad, Inshad Jum'h, Nabil Alaqtash, and A. A. Bani-Salameh. "Optical properties of transparent PMMA-PS/ZnO NPs polymeric nanocomposite films: UV-Shielding applications." Materials Research Express 6, no. 12 (2020): 126446.

[6] Bhadra, S.; Singha, N.K.; Khastgir, D. Polyaniline by new miniemulsion polymerization and the effect of reducing agent on conductivity. Synth. Met. 2006, 156, 1148–1154.

[7] Vizza, M., Pappaianni, G., Giurlani, W., Stefani, A., Giovanardi, R., Innocenti, M., & Fontanesi, C. (2021). Electrodeposition of Cu on PEDOT for a Hybrid Solid-State Electronic Device. Surfaces, 4(2), 157-168.

[8] Gula, S., & Bilal, S. (2013, June). Synthesis and characterization of processable polyaniline salts. In Journal of Physics: Conference Series (Vol. 439, No. 1, p. 012002). IOP Publishing.

[9] J. Tauc (Ed.), Amorphous and Liquid Semiconductors. Plenum, New York, 1974.

[10] Bormashenko, E., Pogreb, R., Sutovski, S., Shulzinger, A., Sheshnev, A., Izakson, G., & Katzir, A. (2004). Infrared optics applications of thin polyaniline emeraldine base films. Synthetic metals, 140(1), 49-52.

[11] Pascual, A.A., 2003. Semi-empirical computation of molecular properties affecting the electrical conductivity of polyaniline and polypyrrole as influenced by doping. (Undergraduate thesis), University of the Philippines, Los Baños.

[12] Sajeev, U. S., Mathai, C. J., Saravanan, S., Ashokan, R. R., Venkatachalam, S., & Anantharaman, M. R. (2006). On the optical and electrical properties of rf and ac plasma polymerized aniline thin films. Bulletin of Materials Science, 29(2), 159-163.

[13] Bandgar, D. K., Khuspe, G. D., Pawar, R. C., Lee, C. S., & Patil, V. B. (2014). Facile and novel route for preparation of nanostructured polyaniline (PANi) thin films. Applied Nanoscience, 4(1), 27-36.

[14] SL, P., MA, C., SG, P., & Shashwati, S. (2012). Effect of camphor sulfonic acid doping on structural, morphological, optical and electrical transport properties on polyaniline-ZnO nanocomposites. Soft Nanoscience Letters, 2012.

[15] J.P. Pouget, C.-H. Hsu, A.G. MacDiarmid, A.J. Epstein, Structural investigation of metallic PAN-CSA and some of its derivatives, Synth. Met. 69 (1995) 119.

[16] D. Djurado, Y.F. Nicolau, I. Dalsegg, E.J. Samuelsen, X-ray scattering study of CSA protonated polyaniline films and powders, Synth. Met. 84 (1997) 121-122.

[17] Al-Gharram, M., Jum'h, I., Telfah, A., & Al-Hussein, M. (2021). Highly crystalline conductive electrodeposited films of PANI-CSA/CoFe2O4 nanocomposites. Colloids and Surfaces A: Physicochemical and Engineering Aspects, 628, 127342.

[18] M. Sniechowski, R. Borek, K. Piwowarczyk, W. Luzny, New structural model of PANI/CSA conducting polymer system obtained by molecular dynamics simulations, Macromol. Theory Simul. 24 (2015) 284–290.

[19] M. Al-Hussein, W.H. de Jeu, L. Vranichar, S. Pispas, N. Hadjichristidis, T. Itoh, J. Watanabe, Bulk and thin film ordering in side-chain liquid-crystalline/ amorphous diblock copolymers: the role of chain length!bulk and thin film ordering in side-chain liquid-crystalline/amorphous diblock copolymers: the role of chain length, Macromolecules 37 (2004) 6401–6407.